

Equivalence between simple multilayered and homogeneous laboratory-based rheological models in planetary science

Yeva Gevorgyan,^{1,2*} Isamu Matsuyama,¹ and Clodoaldo Ragazzo²

¹Lunar and Planetary Laboratory, University of Arizona, Tucson, AZ 85721, USA

²Instituto de Matemática e Estatística, Universidade de São Paulo, 05508-090 São Paulo, SP, Brazil

Accepted 2023 May 14. Received 2023 April 17; in original form 2023 March 07

ABSTRACT

The goal of this work is to investigate under which circumstances the tidal response of a stratified body can be approximated by that of a homogeneous body. We show that any multilayered planet model can be approximated by a homogeneous body, with the same dissipation of tidal energy as a function of the excitation frequency, as long as the rheology of the homogeneous model is sufficiently complex. Moreover we provide two straightforward methods for finding the parameters of the homogeneous rheology that would exhibit the same tidal response as the layered body. These results highlight the fact that the two models cannot be distinguished from each other only by the measurement of the second degree tidal Love number and quality factor, and that we do not need the complexity of the multilayer planet model in order to estimate its tidal dissipation. The methodology promises a great simplification of the treatment of multilayered bodies in numerical simulations because the treatment of a homogeneous body—even with a complex rheological model—can be computationally better handled than that of a multilayered planet.

Key words: Moon – planets and satellites: interiors – methods: analytical

1 INTRODUCTION

Since the discovery of the first exoplanet by [Mayor & Queloz \(1995\)](#) over 5000 exoplanets and almost 4000 exoplanetary systems have been identified and cataloged, hence it is becoming necessary to consider tidal interactions in exoplanetary systems. The tidal response of a planet depends on the timescale of the perturbation and on the rheological properties of its interior (i.e., elasticity, density, and viscosity) ([Bagheri et al. 2022](#)). Many moons and planets within the solar system exhibit a stratified internal structure, as confirmed by seismic and moment of inertia data. For the Earth, for example, the multilayered Preliminary Reference Earth model (PREM) is widely accepted ([Dziewonski & Anderson 1981](#)). Bodies like the Moon ([Harada et al. 2014](#)) and Mercury ([Goossens et al. 2022](#)) are also known to have a stratified structure. Some icy moons have clear evidence of subsurface oceans and consequently stratified internal structure, e.g. Enceladus ([Thomas et al. 2016](#)), Europa ([Carr et al. 1998](#)), Titan ([Iess et al. 2012](#)). Several models that account for the layered internal structure of these bodies were proposed ([Matsuyama 2014](#); [Matsuyama et al. 2018](#); [Folonier & Ferraz-Mello 2017](#); [Boué et al. 2017](#); [Bolmont et al. 2020](#); [Ragazzo et al. 2022](#)). The stratified internal structure of the Solar System bodies suggests complex internal structure for the extrasolar planets as well. While the observational data in our Solar System is relatively abundant, we have few observational constraints for extrasolar planets. Stratified models are usually complex and require to fit numerous parameters from the observational data. Models with few adjustable parameters can be a good alternative to study exoplanets with scarcity of data, or to investigate

rotational and orbital evolution of nearby objects, since considering a multilayered structure does not significantly impact the rotational states of the planets ([Walterová & Běhounková 2017](#)). One possible approach is to model the otherwise stratified body after an effective homogeneous rheological model ([Ragazzo & Ruiz 2017](#); [Gevorgyan et al. 2020](#); [Gevorgyan 2021](#)). The rheological models used are usually the ones proposed based on visco-elastic behavior of planetary materials in laboratory conditions, such as Maxwell, Voigt, Burgers, Andrade ([Andrade 1910](#)), Sundberg-Cooper ([Sundberg & Cooper 2010](#)) or their combinations. The natural question is to what extent stratified bodies can be modeled with homogeneous rheological models.

The use of a homogeneous body to approximate the tidal response of a multilayered structured body, was recently addressed in [Bolmont et al. \(2020\)](#). The authors conclude that it is possible to approximate the response of a multilayered planet by that of a homogeneous planet for purely rocky bodies, but not for planets with both rocky and icy layers due to the large differences in material properties (in particular the viscosity), which results in additional peaks in the frequency dependence of tidal dissipation. However, [Gevorgyan \(2021\)](#) show that the tidal response of a planet with large viscosity variations between layers can in fact be approximated by a homogeneous body, if the rheology of the homogeneous model is slightly more complex than the one used in [Bolmont et al. \(2020\)](#).

In this work, we revisit the problem of approximating the tidal response of a stratified body by that of a homogeneous body. We show that any multilayered body can be approximated by a homogeneous body, with the same dissipation of tidal energy as a function of the excitation frequency, as long as the rheology of the homogeneous model is sufficiently complex.

* E-mail: yeva@ime.usp.br (YG)

The paper is structured as follows: In Section 2, we shortly discuss the dissipation models used in the paper. In Section 2.2, we propose a way to associate a homogeneous rheology to a given stratified celestial object. In Section 3, we provide a recipe to simplify the homogeneous rheology preserving the rheological behavior in an interval of frequencies of interest. In a second step we show that from the homogeneous model with complex rheology we may extract a "minimal model" which is much simpler but still reproduces the rheological behavior of the multilayered body with accuracy. Finally, In the Section 4, we summarize the main results and discuss the implications of our findings.

2 DISSIPATION MODELS

We consider a deformable body orbiting a point-like perturbing body and experiencing tidal deformations under its influence. Tidal deformation of a celestial body results in both vertical and horizontal displacement of its surface and in the ensuing perturbation of its gravitational field, which is described in terms of Love numbers. The Love numbers depend on the timescale of the perturbation and on the rheological properties of the interior (i.e., elasticity, density, and viscosity). In particular, the degree-2 tidal Love number k_2 (Love 1911) quantifies the ability of a celestial body to respond to degree-2 tidal forcing. For a perfectly elastic body the deformation is instantaneous, and the tidal bulges are aligned with the direction of the perturbing body. There is no tidal evolution in this case. However, for a real body, the response is never perfectly elastic and part of the response is dissipative, resulting in a delay or lag in the deformation. Here we are interested in comparing the dissipative behavior of a body modeled assuming a homogeneous or stratified interior structure.

Gevorgyan et al. (2020) obtained an analytic formula for the tidal energy dissipation rate of a body in 1:1 spin-orbit resonance on a slightly eccentric planar orbit in the presence of forced librations. Ignoring forced libration contributions (here we are not interested in this contribution, which could be added to the problem if needed), we obtain the commonly used expression for the time- and volume-averaged tidal energy dissipation rate (e.g., Poirier et al. (1983), Eq. 24; Segatz et al. (1988), Eq. 13)

$$\frac{\Delta E}{T} = -\Im[k_2(i\omega)] \frac{(nR)^5}{G} \left(\frac{m_2}{m_1 + m_2} \right)^2 \times \frac{21}{2} e^2, \quad (1)$$

where $k_2(i\omega)$, ω , n , R , G , m_1 , m_2 , and e are, respectively, the 2nd-degree tidal Love number, tidal forcing frequency, mean rotation rate, mean radius, gravitational constant, mass of the deformable body, mass of the perturbing body, and orbit eccentricity. The frequency-dependent part of the dissipation rate is encoded in the imaginary part of the tidal Love number, $k_2(i\omega)$, hence we will use it instead of the dissipation rate in the paper.

2.1 Dissipation in a stratified body

The tidal response of a stratified body and the corresponding Love numbers can be found by solving the mass conservation, momentum conservation, and Poisson equations. We use the classical propagator matrix method to solve these equations (e.g. Sabadini et al. 2016). The solid core is treated as in Matsuyama et al. (2018, Appendix A). Each layer is assumed to be either solid with linear viscoelastic rheology or liquid and inviscid. Viscoelastic layers are assumed to have a Maxwell rheology characterized by an elastic shear modulus and a viscosity. Liquid layers can be treated using the method of Jara-Oru 

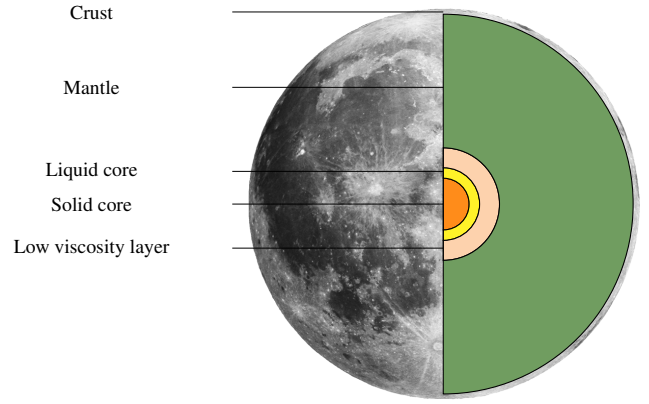


Figure 1. Moon internal structure.

& Vermeersen (2011), or by assuming a viscoelastic layer with shear modulus approaching zero, which yields virtually the same results.

We consider the specific case of the Moon to illustrate the theoretical results below, assuming a 5-layer interior structure in Figure 1 consisting of a solid core, liquid core, low viscosity layer, mantle and crust, based on mass, moment of inertia, and gravity constraints (Matsuyama et al. 2016), as summarized in Table 1. The solid core radius and density were adjusted to satisfy to mass and moment of inertia constraints. The presence of a low viscosity layer at the base of the mantle is consistent with the seismic constraints obtained by Weber et al. (2011); however, the seismic model of Garcia et al. (2011) does not include such a layer. Harada et al. (2014) illustrated that a low viscosity layer at the base of the mantle can explain the frequency dependence of the tidal quality factor Q^1 (Williams & Boggs 2015) assuming a simple Maxwell rheology. Nimmo et al. (2012) attribute the observed frequency dependence to an absorption band due to grain boundary sliding. Although authors were able to fit the monthly Q and k_2 , the model that they used to obtained the correct sign of the Q 's slope did not match k_2 . Recently, Walterov  et al. (2023) concluded that the available selenodetic tidal parameters are insufficient to distinguish a weak basal layer above the lunar core from the manifestation of elastically accommodated GBS in the mantle.

The tidal quality factor Q is constrained at multiple forcing periods by lunar laser ranging (Williams & Boggs 2015): $Q = 38 \pm 4$ at 1 month, $Q = 41 \pm 9$ at 1 year, $Q \geq 74$ at 3 years, and $Q \geq 58$ at 6 years. Although the large uncertainties allow for a Q decreasing (i.e. more dissipation) with forcing period, the mean values of the empirical Q seems to increase (i.e. less dissipation) with forcing period. We adjust the low viscosity layer rigidity and viscosity to satisfy the tidal Q constraints. This requires viscosities $\sim 10^{16}$ Pa s, which is significantly smaller than typical Earth's mantle viscosities, as found in previous studies (Harada et al. 2014; Matsumoto et al. 2015). Red dotted lines in Figure 2 show the imaginary and real parts of k_2 and the quality factor Q as a function of frequency for the interior structure summarized in Table 1. The points with error bars in Figure 2 are the observational constraints.

¹ The quality factor is defined as minus the ratio between the real and the imaginary parts of the Love number.

Table 1. Lunar interior structure parameters.

The layer	Outer radius (km)	Density (kg/m ³)	Rigidity (GPa)	Viscosity (Pa s)
Solid core	213.517	7720.16	40	10 ²¹
Liquid core	325	6700	10 ⁻¹⁰	1
Low viscosity layer	500	3800	60	5 × 10 ¹⁶
Mantle	1697.15	3356	62.5	10 ²¹
Crust	1737.15	2735	15	10 ²³

We assume a 5-layer interior structure based on the mass, moment of inertia, and gravity constraints (Matsuyama et al. 2016, Table 2). The core density is adjusted to satisfy the mass and moment of inertia constraints. All parameters are within the uncertainties in Matsuyama et al. (2016). The core and mantle viscosity of 10²¹ Pa s is representative of Earth’s mantle, and the crust viscosity of 10²³ Pa s is representative of Earth’s lithosphere.

2.2 Dissipation in a homogeneous body

Suppose we are given a spherically symmetric body with interior stratification. Each layer of the body is homogeneous, incompressible, and with Maxwell rheology. We will show the existence of a hypothetical homogeneous body with the same response to tidal forcing as the multilayered body. More precisely we will show that the Love numbers k_2 of both the multilayer and the homogeneous bodies have the same dependence on the frequency of tidal forcing. The rheology of the homogeneous body has to be sufficiently complex and it can be either given by a generalized Maxwell model or by a generalized Voigt model.

The degree-2 tidal Love number in the frequency domain (the domain of the Laplace transform $s \in \mathbb{C}$) is related to a complex compliance $C(s)$ of the whole system defined as (see Mathews et al. (2002) paragraph [21])

$$k_2(s) := \left(\frac{3I_o G}{R^5} \right) C(s), \quad (2)$$

where I_o is the mean moment of inertia (the dimension of $\frac{3I_o G}{R^5}$ is 1/time² and the dimension of $C(s)$ is time²). A similar expression for $k_2(\omega)$ was obtained in Correia et al. (2018). If the inertia of deformation is neglected, as assumed in this paper, then

$$k_2(i\omega) = \frac{3GI_o}{R^5} \frac{1}{\gamma + \hat{f}^{-1}(i\omega)}, \quad (3)$$

where $\hat{f}(i\omega)$ is the complex compliance of the viscoelastic element and γ is a gravitational rigidity parameter related to the fluid Love number k_f as (Ragazzo 2020, Eq. 1.8)

$$\gamma = \frac{3I_o G}{R^5} \frac{1}{k_f}. \quad (4)$$

Fluid Love number can be approximated by $k_f \approx \frac{3}{2} \left(\frac{R_I}{R} \right)^5$, where inertial radius is defined by $R_I = \sqrt{\frac{5I_o}{2m}}$.

2.2.1 The generalized Maxwell model

The following is true for the complex compliance of the generalized Maxwell model² in Figure 3:

² The elastic parameters $\alpha, \alpha_1, \dots, \alpha_n$ have dimension of 1/time² and the viscosity parameters $\eta, \eta_1, \dots, \eta_n$ have dimension of 1/time. To go to the usual dimensions of Pa and Pa·s we should multiply them by the rescaling constant $\frac{15}{152\pi} \frac{mM_{\text{Moon}}}{R}$ (for details see (Correia et al. 2018))

a) The complex compliance of the model is given by (Bland 2016)

$$C^{-1}(s) = \alpha + \eta s + \sum_{i=1}^n \left(\frac{1}{\alpha_i} + \frac{1}{\eta_i s} \right)^{-1}. \quad (5)$$

b) Straightforward algebraic manipulations allow us to rewrite the complex compliance in the form

$$C(s) := \frac{P_2(s)}{P_1(s)} = \frac{(\eta_1 \dots \eta_n)(s + \omega_1) \dots (s + \omega_n)}{P_1(s)}, \quad (6)$$

where $\omega_i^{-1} = \eta_i/\alpha_i$ is the Maxwell time of the i -th Maxwell element,

$$P_1(s) = (\eta_1 \dots \eta_n) \left\{ (\eta s + \alpha) \prod_{i=1}^n (\omega_i + s) + s \sum_{i=1}^n \alpha_i \prod_{j \neq i} (\omega_j + s) \right\}, \quad (7)$$

and where for later convenience we consider the ω_i ordered like $0 < \omega_1 < \omega_2 < \dots < \omega_n$.

c) $P_1(s)$ is a polynomial of degree $n + 1$ with distinct real roots and can be written as

$$P_1(s) = \eta (\eta_1 \dots \eta_n) (s - s_1) \dots (s - s_{n+1}), \quad (8)$$

where s_i is the inverse of the relaxation time of mode i .³ From expression (7) we see that $\text{sgn}\{P_1(-\omega_i)P_1(-\omega_{i+1})\} = \text{sgn}\{(-1)^i(-1)^{i+1}\}$ is negative, $P_1(0) = \alpha(\omega_1 \omega_2 \dots \omega_n) > 0$ and $\text{sgn}\{P_1(-\infty)\} = \text{sgn}\{(-1)^{n+1}\}$ is opposite to $\text{sgn}\{P_1(-\omega_n)\}$, meaning that $P_1(s)$ changes sign $n + 1$ times along the negative real line. Since a continuous function that changes sign inside an interval has a root in that interval (Bolzano’s theorem), $P_1(s)$ has a root in each of the intervals $(-\infty, -\omega_n)$, $(-\omega_n, -\omega_{n-1})$, \dots , $(-\omega_1, 0)$, totaling $n + 1$ distinct negative real roots. The roots of P_1 and P_2 are related by (see Figure 4)

$$0 < -s_1 < \omega_1 < -s_2 < \omega_2 < \dots < -s_n < \omega_n < -s_{n+1}. \quad (9)$$

d) The decomposition in partial fractions of $C(s)$ is given by

$$C(s) = \frac{1}{\eta} \left(\frac{A_1}{s - s_1} + \dots + \frac{A_{n+1}}{s - s_{n+1}} \right), \quad (10)$$

³ The compliance $C(s)$ can be viewed as the transfer function of the homogeneous linear system composed by the elements of the generalized Maxwell rheology (Ragazzo et al. 2022, Eq. 5.31). The poles s_i of $C(s)$ are, therefore, the roots of the characteristic equation, i.e., the eigenvalues of the linear system.

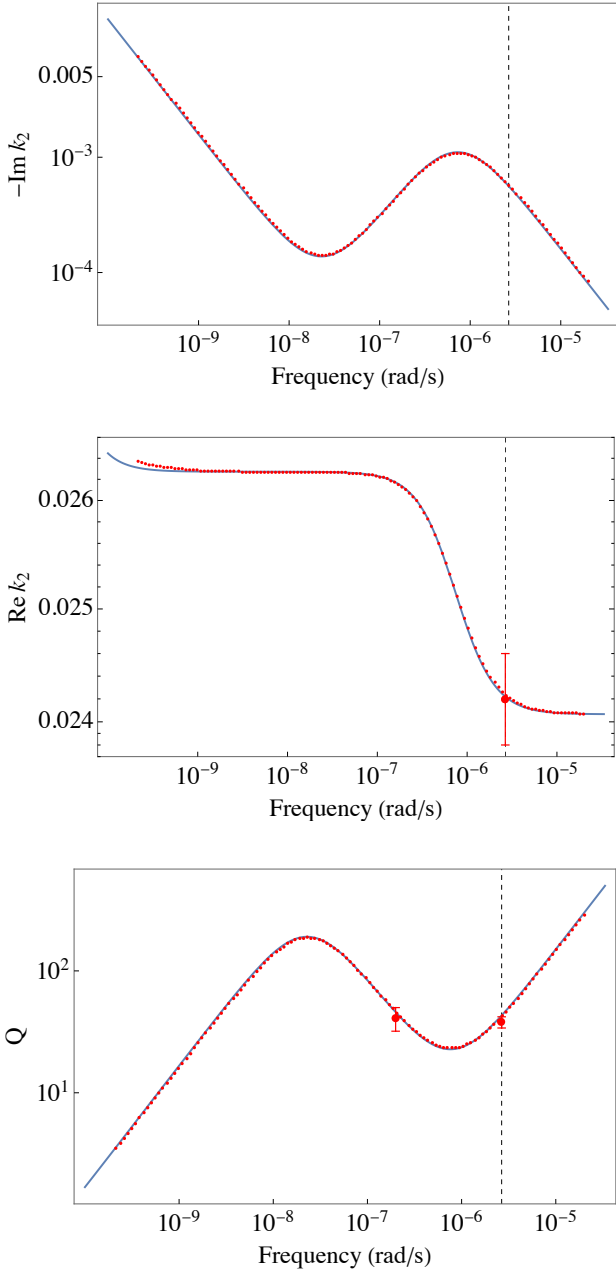


Figure 2. Tidal Love number and quality factor dependence on frequency for the Moon. Red dotted lines show the imaginary and real parts of k_2 and the quality factor Q as a function of frequency for the interior structure summarized in Table 1. The red points with error bars are the observational constraints. Blue solid lines are obtained with homogeneous rheological models in Sections 3.1 and 3.2.

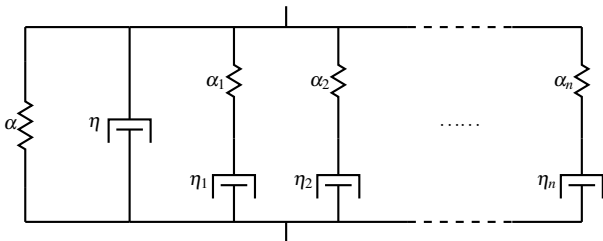


Figure 3. The generalized Maxwell model.

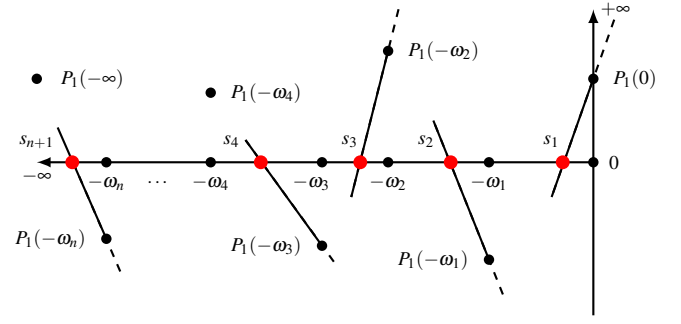


Figure 4. Distribution of poles and zeros of the complex compliance. The figure depicts the case for n odd.

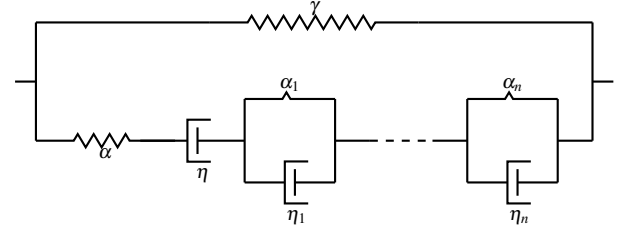


Figure 5. The generalized Voigt model.

where

$$A_i = \frac{1}{1/\eta} \times \frac{P_2(s_i)}{P_1'(s_i)} = \frac{(s_i + \omega_1) \dots (s_i + \omega_n)}{\prod_{j \neq i}^{n+1} (s_i - s_j)} > 0, \quad (11)$$

where the positivity of A_i comes from (9), which gives $\text{sgn}\{P_2(s_i)\} = \text{sgn}\{(-1)^{i-1}\} = \text{sgn}\{P_1'(s_i)\}$, and $\sum_i A_i = 1$, since from equations (6) and (8) we have $\lim_{s \rightarrow \infty} sP_2(s)/P_1(s) = 1/\eta$ and from equation (10) we have $\lim_{s \rightarrow \infty} sC(s) = (1/\eta) \sum_i A_i$, furnishing the result.

The second degree tidal Love number can be rewritten using equations (2) and (10), as

$$k_2(s) = \left(\frac{3I_0 G}{R^5} \right) \times \frac{1}{\eta} \left(\frac{A_1}{s - s_1} + \dots + \frac{A_{n+1}}{s - s_{n+1}} \right). \quad (12)$$

2.2.2 The generalized Voigt model

The following is true for the complex compliance of the generalized Voigt model with the additional spring γ in parallel as in Figure 5:

a) The complex compliance of the model is given by (Bland 2016)

$$C^{-1}(s) = \gamma + \left\{ \frac{1}{\alpha} + \frac{1}{\eta s} + \sum_{i=1}^n \frac{1}{\alpha_i + s\eta_i} \right\}^{-1} \quad (13)$$

and

$$C(s) := \frac{1}{\alpha + \gamma} + C_v(s), \quad (14)$$

where $C_v(s)$ is the viscous compliance as defined in (Sabadini et al. 2016, equation (1.192)). The following limits hold:

$$\lim_{s \rightarrow \infty} C(s) = \frac{1}{\gamma + \alpha} \quad \text{and} \quad \lim_{s \rightarrow \infty} sC_v(s) = \frac{\alpha^2}{(\gamma + \alpha)^2} \left(\frac{1}{\eta} + \sum_{i=1}^n \frac{1}{\eta_i} \right)$$

(15)

b) Straightforward algebraic manipulations allow us to rewrite the viscous compliance in the form

$$C_v(s) := \frac{P_2(s)}{P_1(s)}, \quad (16)$$

where

$$P_2(s) = \alpha^2(\eta_1 \dots \eta_n) \left\{ \left(\prod_{i=1}^n (\omega_i + s) + \eta s \sum_{i=1}^n \frac{1}{\eta_i} \prod_{j \neq i}^n (\omega_j + s) \right) \right\}, \quad (17)$$

$$\begin{aligned} P_1(s) &= (\alpha + \gamma)(\eta_1 \dots \eta_n) \\ &\times \left\{ (\alpha \eta s + \gamma \eta s + \gamma \alpha) \prod_{i=1}^n (\omega_i + s) + \gamma \alpha \eta s \sum_{i=1}^n \frac{1}{\eta_i} \prod_{j \neq i}^n (\omega_j + s) \right\} \\ &= (\alpha + \gamma)(\eta_1 \dots \eta_n) \left\{ \eta(\alpha + \gamma) s \prod_{i=1}^n (\omega_i + s) + \frac{\gamma}{\alpha} P_2(s) \right\}, \end{aligned} \quad (18)$$

$\omega_i^{-1} = \eta_i / \alpha_i$ is the characteristic time of i -th Kelvin-Voigt element, and for later convenience we consider the ω_i ordered like $0 < \omega_1 < \omega_2 < \dots < \omega_n$.

c) $P_2(s)$ is a polynomial of degree n with distinct negative real roots and can be written as

$$P_2(s) = \alpha^2(\eta_1 \dots \eta_n) \left(1 + \eta \sum_{i=1}^n \frac{1}{\eta_i} \right) (s - q_1) \dots (s - q_n). \quad (19)$$

The roots of $P_2(s)$ are related to the inverse characteristic times of Kelvin-Voigt elements as

$$0 < -q_1 < \omega_1 < -q_2 < \omega_2 < \dots < -q_n < \omega_n. \quad (20)$$

$P_1(s)$ is a polynomial of degree $n+1$ with distinct real roots and can be written as

$$P_1(s) = (\alpha + \gamma)^2 \eta (\eta_1 \dots \eta_n) (s - s_1) \dots (s - s_{n+1}). \quad (21)$$

The roots of $P_1(s)$ are related to the inverse characteristic times of Kelvin-Voigt elements as

$$0 < -s_1 < -q_1 < -s_2 < -q_2 < \dots < -s_n < -q_n < -s_{n+1}. \quad (22)$$

d) The decomposition in partial fractions of $C_v(s)$ is given by

$$C_v(s) = \frac{\alpha^2}{(\gamma + \alpha)^2} \left(\frac{1}{\eta} + \sum_{i=1}^n \frac{1}{\eta_i} \right) \left(\frac{A_1}{s - s_1} + \dots + \frac{A_{n+1}}{s - s_{n+1}} \right), \quad (23)$$

where

$$A_i = \frac{1}{\frac{\alpha^2}{(\gamma + \alpha)^2} \left(\frac{1}{\eta} + \sum_{i=1}^n \frac{1}{\eta_i} \right)} \times \frac{P_2(s_i)}{P_1'(s_i)} = \frac{(s_i - q_1) \dots (s_i - q_n)}{\prod_{j \neq i}^{n+1} (s_i - s_j)} > 0 \quad (24)$$

and $\sum_{i=1}^{n+1} A_i = 1$. The facts presented above can be obtained if we proceed in a manner similar to that in Subsection 2.2.1 for the generalized Maxwell model.

The second degree tidal Love number can be rewritten using equations (2), (14) and (23), as

$$\begin{aligned} k_2(s) &= \left(\frac{3I_0 G}{R^5} \right) \\ &\times \left(\frac{1}{\alpha + \gamma} + \frac{\alpha^2}{(\gamma + \alpha)^2} \left(\frac{1}{\eta} + \sum_{i=1}^n \frac{1}{\eta_i} \right) \left(\frac{A_1}{s - s_1} + \dots + \frac{A_{n+1}}{s - s_{n+1}} \right) \right). \end{aligned}$$

(25)

The only dynamical difference between generalized Voigt and generalized Maxwell models is the asymptotic behavior at high frequencies, i.e. as $|s| \rightarrow \infty$. At high frequencies, a body with a generalized Voigt rheology behaves as a purely elastic body while one with a generalized Maxwell rheology behaves as a rigid body.

Note that in the limit $n \rightarrow \infty$, a generalized Voigt rheology is equivalent to an Andrade or a Sundberg-Cooper rheology, frequently used to model otherwise stratified moons and planets (Gevorgyan et al. 2020; Gevorgyan 2021).

2.3 Normal modes of stratified incompressible rheological models

For a stratified body treated as in Section 2.1 the second degree tidal Love number $k_2(s) = N(s)/D(s)$ is a ratio of two polynomials. The roots of the secular equation $D(s) = 0$ and the Love number $k_2(s)$ have the following properties (most of them can be seen in (Sabadini et al. 2016, p. 38) and (Wu & Peltier 1982, the paragraph between equations (55) and (56))):

a) All roots of the secular equation are on the real axis (Tanaka et al. 2006).

b) The secular equation has a finite number of roots, since $D(s)$ is a polynomial.

c) All roots of the secular equation are simple and negative: $0 > s_1 > s_2 > \dots > s_n$, where n is the degree of D , unless for exceptional layered structures, e.g. when the density of a layer is lower than that of the neighboring layer above. The negativity of the roots is a necessary condition for the stability with respect to tidal forcing.

d) The tidal Love number $k_2(s)$ can be decomposed into partial fractions, as in (Sabadini et al. 2016, pg. 105 equation (3.67)):

$$k_2(s) = k_E + \sum_{i=1}^n \frac{r_i}{s - s_i} = k_E + \sum_{i=1}^n \tau_i r_i \frac{1}{\tau_i s + 1}, \quad (26)$$

where k_E is the elastic tidal Love number that characterizes the behavior of the body as $s \rightarrow \infty$, r_i is the amplitude, and $\tau_i = -1/s_i$ is the relaxation time of each mode i .

e) The amplitudes r_i of the modes are positive. Let $s = i\omega$, where $\omega > 0$ is the tidal forcing frequency. Each term in the partial fraction expansion (26) can be decomposed into real and complex parts as

$$r_j \frac{1/\tau_j - i\omega}{\omega^2 + 1/\tau_j^2}. \quad (27)$$

Since $\tau_j > 0$ and $\omega > 0$, the real part is positive (inertial effects were neglected) and the imaginary part is negative (energy is dissipated) if, and only if, the amplitude r_j is positive.

We will say that a body has a *simple layered rheology* if it has finite characteristic times and if its Love number has the properties listed above, which are natural and plausible. A body with finite homogeneous layers, each one with Maxwell rheology, is an example of a body with simple layered rheology. Note that the Maxwell rheology of each homogeneous layer can be replaced by other commonly used rheologies, e.g. Kelvin-Voigt, Burgers, or Andrade. If the number of normal modes is infinite, like for the Andrade model, we would need an infinite number of elements in the generalized Voigt rheology or, alternatively, we could use an effective Andrade or Sundberg-Cooper rheology as in (Gevorgyan 2021).

Since equations (26) and (12) have the same structure if $k_E = 0$ and equations (26) and (25) have the same structure if $k_E > 0$, the following result holds:

The Love number $k_2(s)$ of a body with simple layered rheology is equal to the Love number $k_2(s)$ of a hypothetical homogeneous body with generalized Maxwell or generalized Voigt rheology.

To any given simple layered rheology we can associate either a homogeneous generalized Maxwell or generalized Voigt rheology. The choice of one or another is a matter of convenience since the conditions $k_E = 0$ (generalized Maxwell) or $k_E > 0$ generalized Voigt can be easily changed either by making $\eta = 0$ in the generalized Maxwell rheology, see equation (5) and Figure 3, or by making $\alpha = \infty$ in the generalized Voigt rheology, see equation (14) and Figure 5.

The formulas to go from A_i to r_i are: for the generalized Maxwell model,

$$r_i = \left(\frac{3I_0 G}{R^5} \right) \frac{1}{\eta} \times A_i, \quad (28)$$

and for the generalized Voigt model

$$r_i = \left(\frac{3I_0 G}{R^5} \right) \frac{\alpha^2}{(\gamma + \alpha)^2} \left(\frac{1}{\eta} + \sum_{i=1}^n \frac{1}{\eta_i} \right) \times A_i, \quad (29)$$

$$k_E = \left(\frac{3I_0 G}{R^5} \right) \frac{1}{\gamma + \alpha}.$$

2.4 Normal mode solution for the stratified Moon

Here we present the normal mode decomposition for the stratification we chose for the Moon in Section 2.1. Real and imaginary parts of the second degree tidal Love number are

$$\Re[k_2] = k_E - \sum_{i=1}^N \frac{s_i r_i}{s_i^2 + \omega^2}, \quad \Im[k_2] = - \sum_{i=1}^N \frac{\omega r_i}{s_i^2 + \omega^2}. \quad (30)$$

The normal mode amplitudes, inverse relaxation times and elastic tidal Love number are given in Table 2. The number of modes depends on the stratification choice for the body (Sabadini et al. 2016) and can be relatively large. Large the number of modes requires large number of building elements for the homogeneous rheology, hence we end up with a complex problem to fit the parameters. In the next section we present a way to reduce the number of parameters.

3 SIMPLIFIED HOMOGENEOUS RHEOLOGICAL MODEL

Here we present and compare two procedures to reduce the number of parameters and consequently to simplify the homogeneous rheology: either we find and consider only the dominant modes, which reduces the number of parameters, hence the number of elements in the generalized Maxwell or Voigt model, or we simply fit the Love number frequency dependence curve by hand using a simple rheology with few parameters. The second approach is always feasible, the first one can not be applied if there is not enough information on the internal structure of the body or if the number of dominant modes is too large.

3.1 Simplification by finding dominant modes

The fact that $\sum_{i=1}^n A_i = 1$ and $A_i > 0$, which holds for both the generalized Maxwell and Voigt rheologies, indicates that some of the modes in Sections 2.2.1 and 2.2.2 must be dominant. The same is true for bodies with stratification even when they have infinitely many characteristic times. Indeed, in the limit as $n \rightarrow \infty$ this would

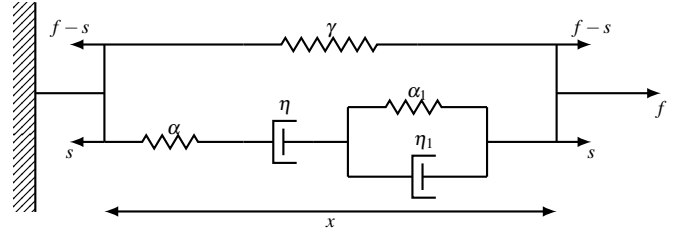


Figure 6. Burgers oscillator. The external force $f(t)$ splits into the force $s(t)$ that acts upon Burgers array plus the force $f(t) - s(t)$ that acts upon the γ spring.

imply that $A_n \rightarrow 0$, and so the smallness of A_i in physically reasonable situations must hold for n large but finite. We show in Appendix A that effective rheologies may be constructed with just dominant amplitudes. Following the procedure in the appendix we conclude that terms marked in red in Table 2 are dominant in the frequency interval from 2×10^{-5} to 2×10^{-10} rad/s, hence we can omit rest of the terms, with no change in tidal Love number frequency dependence, the result is illustrated in Figure A2. The number of relevant modes in the chosen frequency interval is reduced to three. Since we have three dominant modes, we need only two Voigt elements in the generalized Voigt model. We can now fit the parameters of generalized Voigt rheology from the data points 5, 6 and 9 in Table 2, and the equations (29). We obtain the following values for the parameters of generalized Voigt rheology (we will call this rheology 1st rheology): $\gamma = 1.02159$ GPa, $\alpha = 60$ GPa, $\eta = 9.05 \times 10^{20}$ Pa·s, $\alpha_1 = 1050$ GPa, $\eta_1 = 1.66 \times 10^{18}$ Pa·s, $\alpha_2 = 1662$ GPa and $\eta_2 = 1.76 \times 10^{18}$ Pa·s. The fit obtained with these parameters can be seen in Figure 2.

The discussion above shows that a simplification of a rheological model depends on the choice of celestial object and the timescale one is interested in. In this paper we chose the Moon, the second best studied object in the Solar System, to present a procedure to simplify the homogeneous rheology associated to a stratified body. The same procedure can be applied to other bodies.

3.2 Manual simplification

In this section we present a discussion on how to approximate tidal Love number frequency dependence given the plots in Figure 2 or alike for any body. The simplest rheological model able to mimic the dissipation curve in the first plot of Figure 2 is the well-known Burgers rheology in Fig. 6 (Shoji et al. 2013), which we will use to approximate the multilayered Moon by a homogeneous body.

We first see how the dissipation of Burgers model depends on the rheology parameters. The complex compliance for Burgers rheology is (Bland 2016)

$$J(\omega) = \frac{1}{\alpha} + \frac{1}{i\omega\eta} + \frac{1}{\alpha_1 + i\omega\eta_1}, \quad (31)$$

where α , α_1 and η , η_1 have the dimension of s^{-2} and s^{-1} respectively (see Footnote 2). Tidal Love number is given by Equation (3). In Figures 7 and 8 we illustrate how the imaginary and real parts of tidal Love number change with variation of rheology parameters of Burgers model, hence they can be used to finely tune the parameters of Burgers rheology to mimic the dissipative behavior of stratified Moon or any other body.

The best fit is obtained for the following parameters of Voigt rheology (we will call this rheology 2nd rheology) $\alpha = 60$ GPa,

Table 2. The inverse relaxation time, actual and normalized amplitude of each mode i .

i	$s_i(\text{s}^{-1})$	r_i	$\tau_i r_i$
1	-0.1	$2.3156243820 \times 10^{-17}$	$2.3156243820 \times 10^{-16}$
2	-0.1	$9.8181642643 \times 10^{-17}$	$9.8181642643 \times 10^{-16}$
3	-0.1	$5.2900155892 \times 10^{-17}$	$5.2900155892 \times 10^{-16}$
4	-0.1	$8.9387037631 \times 10^{-16}$	$8.9387037631 \times 10^{-15}$
5	$-9.4591261374 \times 10^{-7}$	$8.1074541438 \times 10^{-10}$	0.86×10^{-3}
6	$-6.3419112927 \times 10^{-7}$	$8.5289052773 \times 10^{-10}$	1.35×10^{-3}
7	$-5.0230520036 \times 10^{-10}$	$2.8740137719 \times 10^{-14}$	0.57×10^{-4}
8	$-1.7092727755 \times 10^{-12}$	$6.2186426095 \times 10^{-15}$	3.64×10^{-3}
9	$-1.3953038400 \times 10^{-12}$	$1.5631724063 \times 10^{-12}$	1.05
10	$-1.2295875216 \times 10^{-13}$	$3.4739850530 \times 10^{-14}$	0.283
11	$-2.4641040361 \times 10^{-14}$	$8.1522986569 \times 10^{-17}$	3.31×10^{-3}
12	$-2.4038824848 \times 10^{-14}$	$2.1438046989 \times 10^{-17}$	0.89×10^{-3}
13	$-7.9022589544 \times 10^{-17}$	$4.0680469600 \times 10^{-20}$	0.52×10^{-3}

The elastic tidal Love number is $k_E = 0.024068$. The terms in red are dominant and are the only ones needed to reproduce the tidal Love number frequency dependence seen in Figure A2

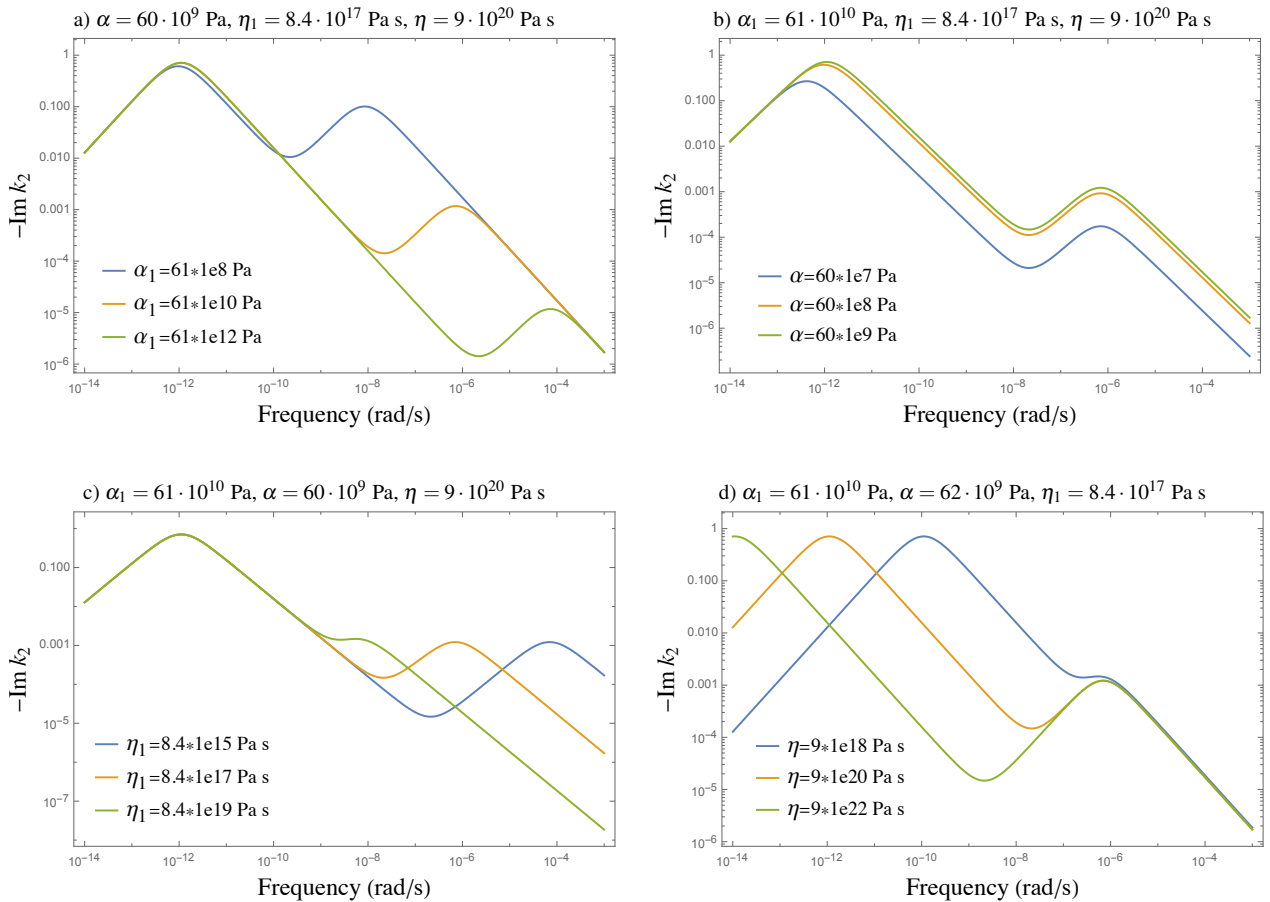


Figure 7. Imaginary part of the degree-2 tidal Love number, which describes dissipation, as a function of frequency for a homogeneous body modeled with Burgers rheology; (a) effect of the Voigt element elasticity α_1 ; (b) effect of the Maxwell element elasticity α ; (c) effect of the Voigt element viscosity η_1 ; (d) effect of the Maxwell element viscosity η .

$\eta = 9.05 \times 10^{20} \text{ Pa} \cdot \text{s}$, $\alpha_1 = 643 \text{ GPa}$ and $\eta_1 = 8.8 \times 10^{17} \text{ Pa} \cdot \text{s}$, and can be seen in Figure 2. The dissipative response assuming the generalized Voigt rheology with two Voigt elements and the parameters obtained in Section 3.1, and that of the Burgers rheology with the parameters described above are indistinguishable from each other. The

choice of simplification method will depend on the problem one is considering, giving preference to the simplest rheological model.

It would be interesting to establish a straightforward connection between the parameters of a stratified body and that of the corresponding homogeneous rheology. For the stratified Moon the dotted lines in Figure 9 are obtained varying the viscosity of the low vis-

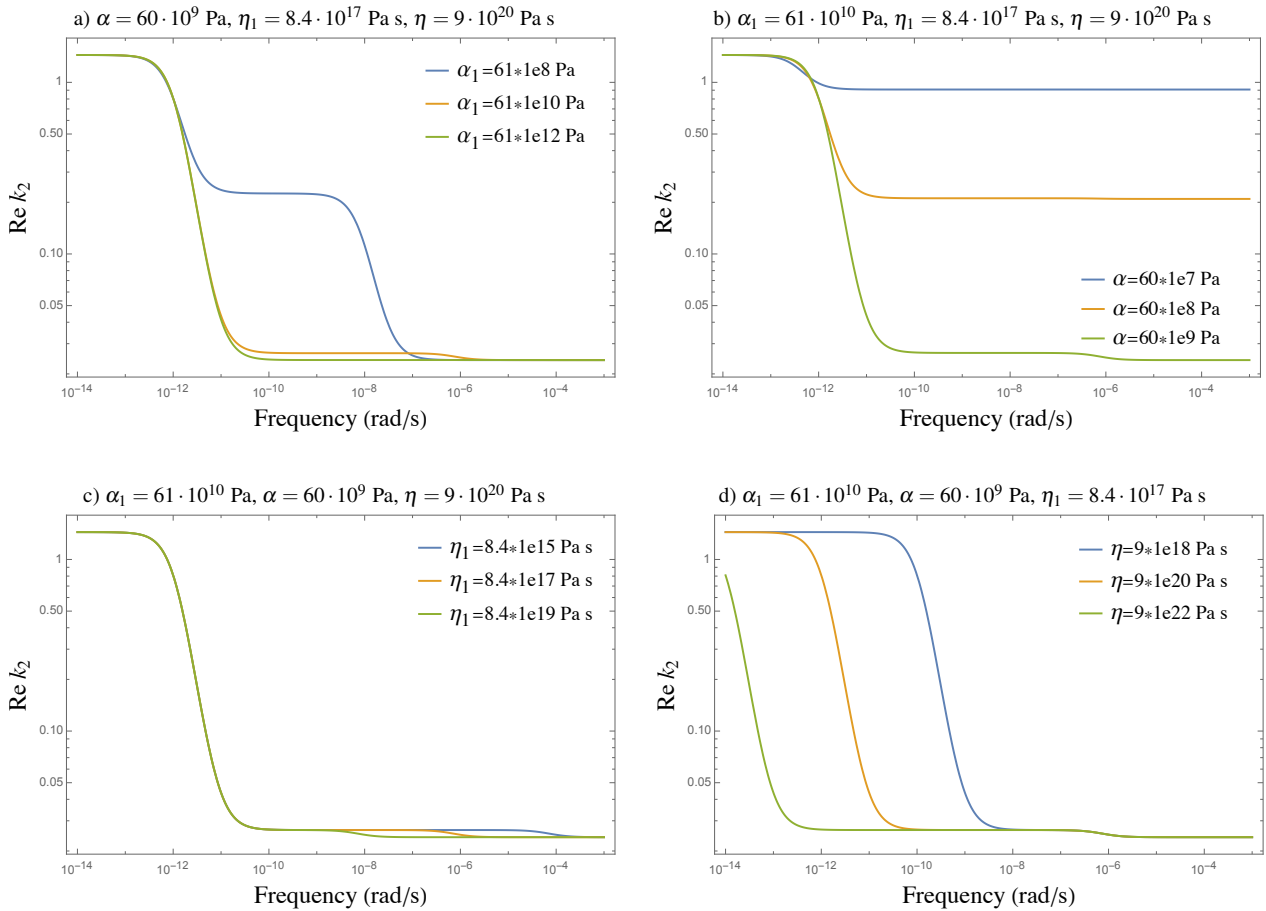


Figure 8. Real part of Love number as a function of frequency for a homogeneous body modeled with Burgers rheology; (a) effect of the Voigt element elasticity α_1 ; (b) effect of the Maxwell element elasticity α ; (c) effect of the Voigt element viscosity η_1 ; (d) effect of the Maxwell element viscosity η .

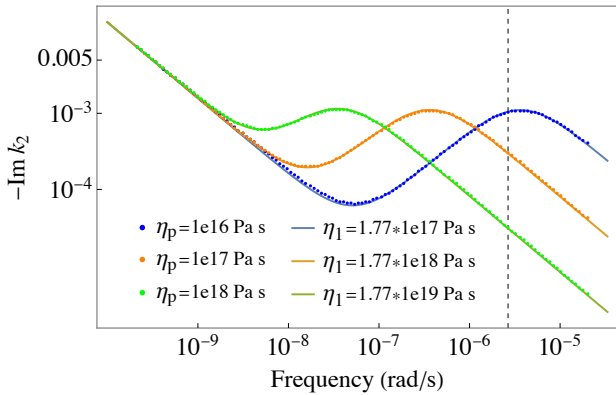


Figure 9. Moon dissipation rate variation due to low viscosity layer viscosity variation. Solid lines are obtained by varying the viscosity of low viscosity layer for the stratified Moon. Dotted lines are obtained by varying the viscosity η_1 of Voigt element in Figure 6 or the viscosities η_1 and η_2 of Voigt elements of 1st rheology.

cosity layer from $10^{16} \text{ Pa} \cdot \text{s}$ to $10^{18} \text{ Pa} \cdot \text{s}$. To mimic the variation in the dissipation rate of the stratified body we vary the viscosities η_1 and η_2 of Voigt elements of 1st rheology from $3.32 \times 10^{17} \text{ Pa} \cdot \text{s}$ to $3.32 \times 10^{19} \text{ Pa} \cdot \text{s}$ and from $3.52 \times 10^{17} \text{ Pa} \cdot \text{s}$ to $3.52 \times 10^{19} \text{ Pa} \cdot \text{s}$, respectively, or the viscosity η_1 of Voigt element of 2nd rheology from $1.77 \times 10^{17} \text{ Pa} \cdot \text{s}$ to $1.77 \times 10^{19} \text{ Pa} \cdot \text{s}$. We then conclude that

the change of the viscosity of the low viscosity layer can be reproduced by a change of the same order of magnitude in the viscosity of Voigt elements of the simplified rheologies.

4 CONCLUSIONS

We revisited the long standing problem of approximating the tidal response of a stratified body by that of a homogeneous body. We show that the frequency dependence of tidal dissipation and the quality factor of a multilayered body can be approximated by that of a homogeneous body with complex rheology. This result highlights the fact that we do not need the complexity of the multilayer planet model in order to estimate its tidal dissipation. On the example of the Moon we illustrate that stratified and homogeneous models cannot be distinguished from each other only by the measurement of second degree tidal Love number and quality factor.

We propose and compare two distinct approaches to associate a simple homogeneous rheology to a given stratified moon or planet. The obtained homogeneous rheology can then be used in tandem with the formalism proposed and developed in (Ragazzo & Ruiz 2017; Correia et al. 2018; Gevorgyan et al. 2020; Ragazzo et al. 2022) to perform a fully three dimensional numerical simulation of the dynamics of a system of many deformable bodies.

It is important to establish a straightforward connection between the parameters of the stratified body and that of the homogeneous rheology. Here we show, on the example of the Moon, that the varia-

tion of viscosity of partial melt layer results in the same order variation of the viscosity of the Voigt elements in generalized Voigt model used to approximate the stratified body. We will revisit the problem to establish more general relations between the parameters in future work.

ACKNOWLEDGEMENTS

The authors thank an anonymous referee for several remarks and many suggestions improving the manuscript. YG is partially supported by FAPESP grants 2019/25356-9 and 2021/09679-2. CR is partially supported by FAPESP grant 2016/25053-8.

DATA AVAILABILITY

The data underlying this paper will be shared on reasonable request to the corresponding author.

REFERENCES

- Andrade E. N. D. C., 1910, Proceedings of the Royal Society of London Series A, **84**, 1
- Bagheri A., et al., 2022, *Advances in Geophysics*, **63**, 231
- Bland D. R., 2016, The Theory of Linear Viscoelasticity. Dover Books on Physics, Dover Publications, <https://books.google.com.br/books?id=YL8zDQAAQBAJ>
- Bolmont E., Breton S. N., Tobie G., Dumoulin C., Mathis S., Grasset O., 2020, *A&A*, **644**, A165
- Boué G., Rambaux N., Richard A., 2017, *Celestial Mechanics and Dynamical Astronomy*, **129**, 449
- Carr M. H., et al., 1998, *Nature*, **391**, 363
- Correia A. C. M., Ragazzo C., Ruiz L. S., 2018, *Celestial Mechanics and Dynamical Astronomy*, **130**, 51
- Dziewonski A. M., Anderson D. L., 1981, *Physics of the Earth and Planetary Interiors*, **25**, 297
- Folonier H. A., Ferraz-Mello S., 2017, *Celestial Mechanics and Dynamical Astronomy*, **129**, 359
- Garcia R. F., Gagnepain-Beyneix J., Chevrot S., Lognonné P., 2011, *Physics of the Earth and Planetary Interiors*, **188**, 96
- Gevorgyan Y., 2021, *A&A*, **650**, A141
- Gevorgyan Y., Boué G., Ragazzo C., Ruiz L. S., Correia A. C. M., 2020, *Icarus*, **343**, 113610
- Goossens S., Renaud J. P., Henning W. G., Mazarico E., Bertone S., Genova A., 2022, *The Planetary Science Journal*, **3**, 37
- Harada Y., Goossens S., Matsumoto K., Yan J., Ping J., Noda H., Haruyama J., 2014, *Nature Geoscience*, **7**, 569
- Iess L., et al., 2012, *Science*, **337**, 457
- Jara-Orué H. M., Vermeersen B. L. A., 2011, *Icarus*, **215**, 417
- Love A. E. H., 1911, Some Problems of Geodynamics. Cambridge University Press
- Mathews P. M., Herring T. A., Buffett B. A., 2002, *Journal of Geophysical Research: Solid Earth*, **107**, ETG
- Matsumoto K., Yamada R., Kikuchi F., Kamata S., Ishihara Y., Iwata T., Hanada H., Sasaki S., 2015, *Geophys. Res. Lett.*, **42**, 7351
- Matsuyama I., 2014, *Icarus*, **242**, 11
- Matsuyama I., Nimmo F., Keane J. T., Chan N. H., Taylor G. J., Wiczcerek M. A., Kiefer W. S., Williams J. G., 2016, *geophysical Research Letters*, **43**, 8365
- Matsuyama I., Beuthe M., Hay H. C. F. C., Nimmo F., Kamata S., 2018, *Icarus*, **312**, 208
- Mayor M., Queloz D., 1995, *Nature*, **378**, 355
- Nimmo F., Faul U. H., Garnero E. J., 2012, *Journal of Geophysical Research (Planets)*, **117**, E09005
- Poirier J. P., Boloh L., Chambon P., 1983, *Icarus*, **55**, 218

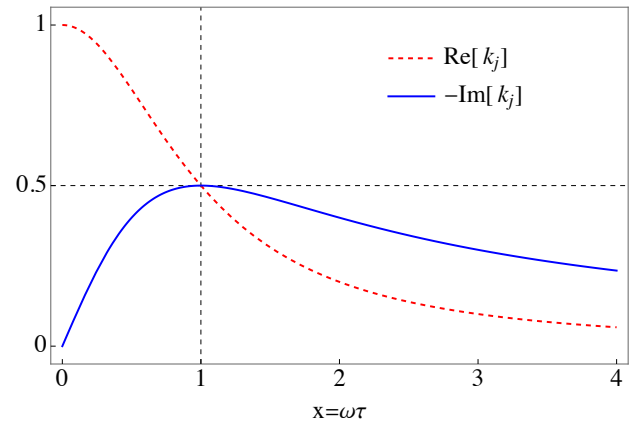


Figure A1. The graphs of the real (red-dashed) and the imaginary (blue) parts of a term (mode) in the partial fraction expansion of $k_2(i\omega)$. The amplitude $r_j\tau_j$ was normalized to one and the angular frequency $x = \omega\tau_j$ was normalized by the relaxation time τ_j of the mode. The maximum of the imaginary part, the point of maximum dissipation of energy, occurs at $x = 1$, which is also the half-width of the real part.

- Ragazzo C., 2020, *São Paulo Journal of Mathematical Sciences*, **14**, 1
- Ragazzo C., Ruiz L. S., 2017, *Celestial Mechanics and Dynamical Astronomy*, **128**, 19
- Ragazzo C., Boué G., Gevorgyan Y., Ruiz L. S., 2022, *Celestial Mechanics and Dynamical Astronomy*, **134**, 10
- Sabadini R., Vermeersen B., Cambiotti G., 2016, *Global dynamics of the Earth*. Springer
- Segatz M., Spohn T., Ross M. N., Schubert G., 1988, *Icarus*, **75**, 187
- Shoji D., Hussmann H., Kurita K., Sohl F., 2013, *Icarus*, **226**, 10
- Sundberg M., Cooper R. F., 2010, *Philosophical Magazine*, **90**, 2817
- Tanaka Y., Okuno J., Okubo S., 2006, *Geophysical Journal International*, **164**, 273
- Thomas P. C., Tajeddine R., Tiscareno M. S., Burns J. A., Joseph J., Lored T. J., Helfenstein P., Porco C., 2016, *Icarus*, **264**, 37
- Walterová M., Běhouňková M., 2017, *Celestial Mechanics and Dynamical Astronomy*, **129**, 235
- Walterová M., Běhouňková M., Efroimsky M., 2023, *arXiv e-prints*, p. arXiv:2301.02476
- Weber R. C., Lin P. Y., Garnero E. J., Williams Q., Lognonné P., 2011, *Science*, **331**, 309
- Williams J. G., Boggs D. H., 2015, *Journal of Geophysical Research (Planets)*, **120**, 689
- Wu P., Peltier W. R., 1982, *Geophysical Journal International*, **70**, 435

APPENDIX A: DOMINANT MODES IN THE NORMAL MODE SOLUTION FOR THE STRATIFIED MOON

The tidal force may be decomposed into harmonic components. Let $\omega > 0$ be the angular frequency of one of these components. The tidal response of the body at frequency ω is determined by $k(i\omega)$. Each term in the expansion (26) has real and imaginary parts given, respectively, by

$$\Re[k_j] = \tau_j r_j \frac{1}{1+x^2}, \quad \Im[k_j] = -\tau_j r_j \frac{x}{1+x^2}, \quad \text{where } x = \omega\tau_j. \quad (\text{A1})$$

The graphs of $\Re[k_j]$ and $\Im[k_j]$ are shown in Figure A1.

Since the maximum of the imaginary part of a mode j is at $\omega = 1/\tau_j$, different modes have their maxima at different points. The modes with larger normalized amplitudes $r_j\tau_j$ are dominant at frequency $\omega = 1/\tau_j$.

If two modes s and g satisfy $r_s \tau_s / (r_g \tau_g) < 1$, then the relative importance of the imaginary part of the modes at a point of maximum $\omega = 1/\tau_s$ of the smaller mode is measured by the ratio

$$\Im[k_s](\tau_s^{-1}) / \Im[k_g](\tau_s^{-1}) = \frac{r_s \tau_s}{2r_g \tau_g} \frac{1 + (\tau_g / \tau_s)^2}{\tau_g / \tau_s}. \quad (\text{A2})$$

For the Moon, in the interval from 2×10^{-5} to 2×10^{-10} rad/s, most relevant modes are 5, 6 and 9 (see Table 2) and $k_2(i\omega)$ is mostly determined by the modes 5, 6 and 9 and by the elastic Love number k_E (see Figure A2).

If two modes s and g satisfy $r_s \tau_s / (r_g \tau_g) \ll 1$ and $\tau_s > \tau_g$, then $r_s \tau_s / (r_g \tau_g) = \Re[k_s](0) / \Re[k_g](0) \geq \Re[k_s](\omega) / \Re[k_g](\omega)$ for all $\omega \geq 0$, and the real part of mode s can be safely neglected. If $r_s \tau_s / (r_g \tau_g) \ll 1$ but $\tau_s < \tau_g$, then $\Re[k_s](\omega) / \Re[k_g](\omega)$ is an increasing function of ω with its maximum at $\omega = \infty$ given by $\frac{r_s \tau_g}{r_g \tau_s}$. The smaller mode s might have some importance at high frequencies.

To illustrate the discussion in the previous paragraphs, we will analyze the effect of the mode 7 in Table 2 on the plots of the real and the imaginary parts of $k_2(i\omega)$ shown in Figure A2. The mode 7 has a normalized amplitude $r_7 \tau_7 = 0.000057$ and a relaxation time $\tau_7 = 2 \times 10^9$ seconds. Compared to the dominant mode 9: $r_7 \tau_7 / (r_9 \tau_9) = 0.000054$ and $\tau_7 / \tau_9 = 1/357$. At the frequency $\omega = 1/\tau_7$, where $\Im[k_7](\omega)$ is maximum, the ratio in equation (A2) is $\Im[k_7](\tau_7^{-1}) / \Im[k_9](\tau_7^{-1}) = 0.01$. The effect of the mode 7 at frequency 5×10^{-10} (rad/sec) is, therefore, 100 times smaller than the effect of the mode 9. Compared to the dominant mode 6: $r_7 \tau_7 / (r_6 \tau_6) = 0.042$ and $\tau_7 / \tau_6 = 1268.4$, consequently the effect of the mode 7 is at least 25 times smaller than the effect of the mode 6 on the real part of $k_2(i\omega)$. This explains why mode 7 can be neglected.

This paper has been typeset from a $\text{\TeX}/\text{\LaTeX}$ file prepared by the author.

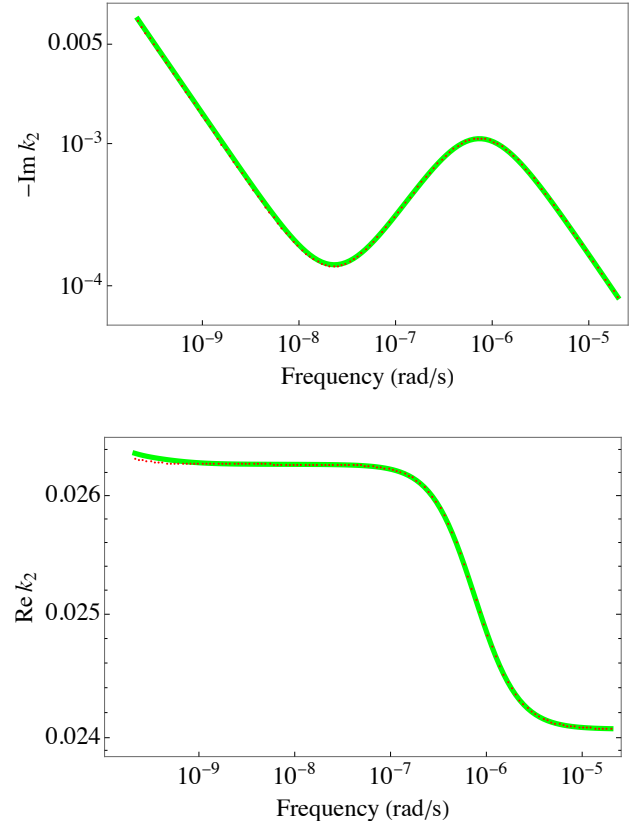


Figure A2. Tidal Love number dependence on frequency for the Moon. The green solid line was plotted using all the terms and the red dotted line was plotted using only the terms highlighted in red terms in Table 2.